PNAS NEXUS

PNAS Nexus, 2025, 4, pgaf189

https://doi.org/10.1093/pnasnexus/pgaf189
Advance access publication 6 June 2025
Research Report

Biophysical basis of tight junction barrier modulation by a pan-claudin-binding molecule

Chinemerem P. Ogbu[a], Mason de las Alas[b,1], Alexandria M. Mandriota[a,1], Xiangdong Liu[a,2], Srajan Kapoor[a,2], Jagrity Choudhury[a,2], Yasmeen N. Ruma[c,d,2], Michael C. Goodman[e,2], Charles R. Sanders[e], Tamir Gonen[c,d,f], Anthony A. Kossiakoff[g], Michael E. Duffey[b] and Alex J. Vecchio[a,*]

[a]Department of Structural Biology, Jacobs School of Medicine and Biomedical Sciences, University at Buffalo, Buffalo, NY 14203, USA
[b]Department of Physiology and Biophysics, Jacobs School of Medicine and Biomedical Sciences, University at Buffalo, Buffalo, NY 14203, USA
[c]Department of Biological Chemistry, David Geffen School of Medicine, University of California, Los Angeles, CA 90095, USA
[d]Howard Hughes Medical Institute, University of California, Los Angeles, CA 90095, USA
[e]Department of Biochemistry and Center for Structural Biology, Vanderbilt University, Nashville, TN 37240, USA
[f]Department of Physiology, David Geffen School of Medicine, University of California, Los Angeles, CA 90095, USA
[g]Department of Biochemistry and Molecular Biology, University of Chicago, Chicago, IL 60637, USA
*To whom correspondence should be addressed: Email: vecchioa@buffalo.edu
[1]M.d.l.A. and A.M.M. contributed equally to this work.
[2]X.L., S.K., J.C., Y.N.R., and M.C.G. contributed equally to this work.
Edited By Michael Fromm

Abstract

Claudins are a 27-member family of membrane proteins that form and fortify specialized cell contacts in endothelium and epithelium called tight junctions. Tight junctions restrict paracellular transport through tissues by forming molecular barriers between cells. Claudin-binding molecules thus hold promise for modulating tight junction permeability to deliver drugs or as therapeutics to treat tight junction–linked disease. The development of claudin-binding molecules, however, is hindered by their physicochemical intractability and small targetable surfaces. Here, we determine that a synthetic antibody fragment (sFab) that we developed binds with nanomolar affinity directly to 10 claudin subtypes and other distantly related claudin family members but not to other tight junction–localized membrane proteins. It does so by targeting the extracellular surfaces of claudins, which we verify by applying this sFab to a model intestinal epithelium and observe that it opens paracellular barriers comparable to a known, but application limited, tight junction modulating protein. This pan-claudin-binding molecule holds potential for both basic and translational applications as it is a probe of claudin and tight junction structure in vitro and in vivo and a tool to modulate the permeability of tight junctions broadly across tissue barriers.

Keywords: claudin, tight junctions, drug delivery, synthetic antibody, membrane proteins

Significance Statement

Tight junctions are cellular structures in animal tissues that restrict the passage of molecules between individual cells. The proteins that regulate tight junction form and function, claudins, are small and membrane-embedded, making them hard to target with therapeutics. Claudin-binding molecules could be used to open tight junction barriers to deliver drugs across tissues or into the brain to treat disease. Here, we characterize a molecule with pan-claudin-binding ability, determine its mechanism of targeting, and show that it opens tight junction barriers in a model of gut epithelium. This molecule or its analogs could have far-reaching applications in a variety of key physiological processes that are controlled by claudins or claudin-like proteins.

Introduction

Claudins are a family of ∼25 kDa membrane-embedded proteins that play the primary role in directing formation of tight junctions and regulating molecular transport through the paracellular spaces between individual cells within epithelial/endothelial sheets (Fig. 1A) (1, 2). The human genome encodes for 27 individual claudin subtypes (1). Although claudins express in all mammalian tissues, individual subtypes have varied and tissue-specific expression patterns and levels that occur at different timepoints throughout tissue development (3). Additionally,

Competing Interest: The authors declare no competing interests.
Received: February 5, 2025. **Accepted:** May 21, 2025

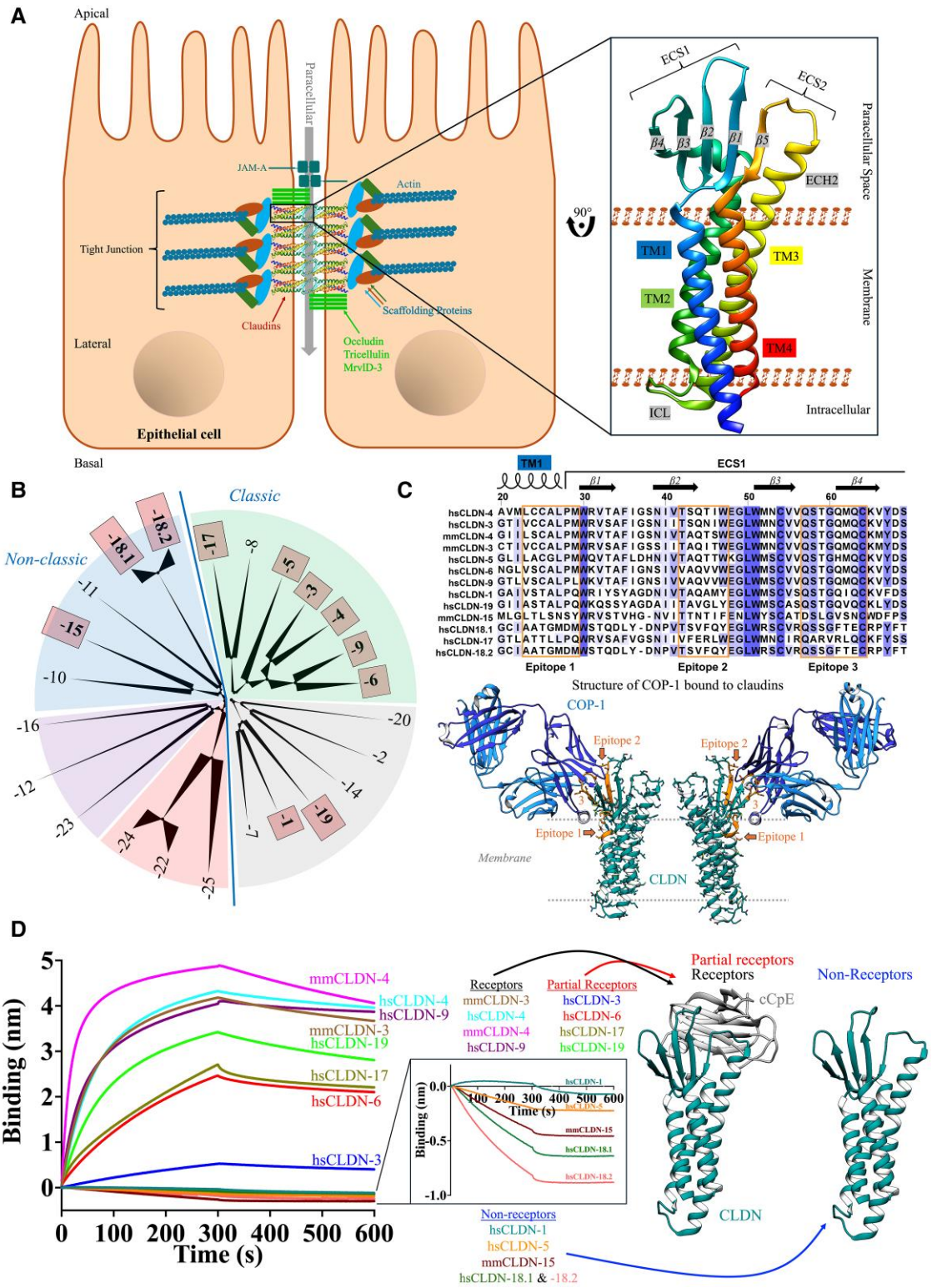

Fig. 1. Sequence, structure, and function classification of claudins. A) Model epithelial bicellular tight junction with zoom-in depicting the 3D structures of claudins. Claudins are colored N terminus (blue) to C terminus (red) and domains of interest are labeled as follows: TM domain, ECS, intracellular loop (ICL), and extracellular helix (ECH). B) Phylogenetic tree of the claudin family highlighting classic vs. nonclassic subtypes and subtypes used in this study (pink box). C) The three known COP-1-binding epitopes on claudins. Sequence alignment of the 13 claudins used in this study with epitopes highlighted (orange box) and arranged in order of sequence identity to hsCLDN-4 COP-1 epitope from highest to lowest. Also shown is the structure of COP-1 (blue) bound the hsCLDN-4 (cyan) with epitopes 1–3 shown (orange). D) Binding of claudins to cCpE from BLI. Association and dissociation phases are 300 s each. Zoom-in shows binding experiment with claudin nonreceptors. Grouping of claudins into three categories based on cCpE receptor capacity from this experiment is shown in relation to structures of claudins alone or claudin/cCpE complexes.

at the molecular level, claudins display unique homo- and heterooligomeric compatibilities with other subtypes, which may be driven by sequence divergences in key regions that define their classic or nonclassic categorization (4). Categorization of claudins into classic (claudin-1–9, 14, 17, 19, 20) or nonclassic (claudin-10–13, 15, 16, 18, 20–27) can differ depending on the length of sequence used and/or the species of focus—murine vs. human, for instance (2, 5–7). The complex yet coordinated interaction network of claudins that constitute a given tissue thus directs its molecular transport properties—as claudin subtype incidence and variety influences the magnitude and morphology of tight junction strands—creating more or less leaky paracellular barriers (1, 8).

Claudins with diverse tissue distributions and paracellular transport functions that are implicated in a wide array of diseases were used in this study. Specifically, claudin-1 is expressed in skin and maintains the epidermal paracellular barrier and is also a receptor for hepatitis C viral (HCV) entry in the liver (9, 10). Claudin-5 is the major regulator of the blood–brain barrier, which forms the protective diffusion layer that limits molecular exchange from the blood to the brain microenvironment and is thus being targeted by claudin-derived peptides, synthetic compounds, monoclonal antibodies, and mutant *Clostridium perfringens* enterotoxin (CpE) to enable drug delivery into the brain (11, 12). Claudin-3 and 4 are highly expressed in the gastrointestinal tract, are barrier-forming claudins, and are receptors for CpE, a common cause of food poisoning (13, 14). Due to CpE interactions with claudins, it has been used to study claudin structure/claudin-receptor interactions and modified to develop mutants and peptidomimetics that modulate tight junctions for drug delivery or target cancers where claudins are overexpressed (15–18). Claudin-6 is expressed during embryonic tissue development where it regulates renal electrolyte homeostasis (19). Although it is not present in normal adult tissues, liver, ovarian, endometrial, testicular, and esophageal cancers overexpress claudin-6, making it a target for solid tumor immunotherapies (20). Claudin-9 is essential for hearing by tuning sodium and potassium ion permeability ratios in subapical tight junctions of sensory hair cells in the inner ear (21). It was identified as a coentry receptor, with claudin-1 and 6, for HCV infection (10). In the kidney, claudin-15, 17, and 19 form diverse ion-selective channels that regulate magnesium and calcium reabsorption, the latter through heterooligomeric interactions with claudin-16 (22–24). Claudin-18 splice variant 18.1 is highly expressed in lung alveolar epithelia where it regulates the alveolar fluid clearance, serves as the primary airway epithelial barrier to aero antigens, and functions as a tumor suppressor attenuating malignant properties including cell proliferation, migration, and invasion (25–27). Claudin-18.2 is normally expressed in differentiated epithelial cells of the gastric mucosa where it blocks paracellular gastric acid leakage from the gastric lumen into the submucosal space (28). It is also observed to be abnormally activated in pancreatic, esophageal, ovarian, and lung tumors (29). Clearly, the vast yet unique functions of individual claudin subtypes play important roles in epithelial and endothelial tissue homeostasis, while dysregulation or misassembly of tight junctions is a hallmark of many diseases.

Due to their roles in formation and maintenance of the tight junction barrier, claudins are attractive targets for the development of claudin-binding molecules, which hold potential to alter tight junction permeability to deliver drugs or to treat diseases linked to tight junction mis- or disassembly (6, 30, 31). To be effective, however, such molecules need to bind the extracellular surfaces of claudins. We have described previously that targeting of claudins is challenging due to their small ~25 kDa masses and having half of this mass being buried within hydrophobic membranes or disordered (32). We concluded that only ~40% (10 kDa) of their extracellular surface is "targetable" for antibody or drug binding. The C-terminal domain of CpE (cCpE) is one of a few molecules established to bind claudin extracellular domains and is known to alter tight junction barrier permeability (33–35). It does so by engaging with both extracellular segments (ECSs) of claudins, where both loops of ECS1 bind the surface of cCpE and a single ECS2 loop penetrates a solvent exposed groove on cCpE (36–40). Within ECS2, the $NPLVA^{153}$ motif is a major driver of high affinity cCpE binding that helps to distinguish CpE receptors from nonreceptors (41–43). However, cCpE only binds with <100 nM affinity to a subset of claudin subtypes and has been shown to be most effective at modulating epithelial barriers after basolateral but not apical delivery (44, 45). Thus, cCpE is tissue-specific and thus may not be a generalizable tight junction modulator. As yet discovered claudin-binding molecules are needed to fill this gap in therapeutic potential.

Recently, we described a synthetic antibody fragment (sFab) termed COP-1 that was developed to target human claudin-4 (hsCLDN-4) (32). Structural analysis of COP-1 bound to hsCLDN-4 revealed that it binds the extracellular domain of hsCLDN-4 in a region different than cCpE and even accesses its transmembrane (TM) domain. Although COP-1 bound hsCLDN-4 best, we showed that it bound homologous claudins with high affinity too. This raised the possibility that COP-1 with its unique binding mode might bind other claudins. Here, we conduct thorough biophysical characterization of COP-1 binding to a diverse selection of claudins from humans, mice, nonvertebrate animals, and distant members of the claudin/PMP22/EMP22/MP20 family to determine its binding mechanism (46, 47). Further, using a tissue system that models small intestinal epithelium and endogenously expresses at least six claudin subtypes, we show that COP-1 reversibly opens tight junction barriers. COP-1 is a newly identified claudin-binding molecule distinct from cCpE whose pan-claudin-binding ability holds potential to increase tight junction permeability broadly across different tissues with diverse claudin expression patterns and barrier properties.

Results

Sequence and structure analysis of claudins used in this study

The 3D structures of claudins have been elucidated and consist of four TM domains, two ECS that span paracellular space, and intracellular N and C termini (Fig. 1A) (32, 36–40, 48). We aligned the sequences of 24 human and three murine claudins to show homology within the family (Fig. S1 and Table S1). Phylogenetic analysis showed that claudins cluster into five distinct groups described previously and broadly can be grouped as classic or nonclassic claudins (Fig. 1B) (5, 6). Thirteen claudins, 10 from humans and 3 from mouse, representing 10 subtypes were used in this study and included human claudin-1, 3, 4, 5, 6, 9, 17, 18.1, 18.2, and 19 (hsCLDN-x) and murine claudin-3, 4, and 15 (mmCLDN-x). These claudins were chosen for their ability to be expressed and purified in vitro and that they were classic or nonclassic claudins or known receptors and nonreceptors of CpE (2, 7, 15, 39, 40, 42).

From the structure of COP-1 bound to hsCLDN-4, three epitopes on claudins were identified that direct COP-1 binding (32). Sequence alignment of residues spanning these epitopes revealed that sequence identity in these epitopes range from 19 to 91% in the 13 claudins of focus compared with hsCLDN-4—with hsCLDN-18.2 being most divergent and hsCLDN-3 being least divergent

(Fig. 1C). Specifically, in epitope 1 we observed 0–89% (avg. 52%); in epitope 2, 17–83% (avg. 42%); and in epitope 3, 29–100% (avg. 74%) sequence identity. We had shown that mutants to residues within these epitopes decrease or increase COP-1s affinity to verify their involvement in binding (32). Having discerned how homologous each subtype was to hsCLDN-4, we embarked on biophysical analyses to discern how claudin sequence divergences effect binding.

Establishing the cCpE receptor capacities of claudins

We cloned, recombinantly expressed, and then biochemically purified the 13 claudins using established methods (39, 40). First, because several claudins had not been functionally characterized before in vitro, we measured all claudin's ability to bind cCpE, a known claudin-binding protein, using biolayer interferometry (BLI). We found that claudins could be grouped into three classes based on estimated equilibrium dissociation constants (K_{Ds}): those that bound cCpE with <20 nM affinity (claudin-3, 4, and 9), those that bound with 20–300 nM affinity (claudin-3, 6, 17, and 19), and those that did not bind cCpE (claudin-1, 5, 15, and 18) (Fig. 1D and Table S2). Interestingly, the human and murine orthologs of claudin-3 fit in two distinct classes. These results showed that the 13 claudins could be classified as cCpE receptors, partial receptors, and nonreceptors, and agreed with binding analyses conducted previously (32, 36, 39, 40, 49).

Since 500 nM claudin was used to scout binding, we validated that nonreceptors did not bind cCpE by increasing claudin concentrations to 2,000 nM. Here, claudin-5, 15, and 18 did not bind cCpE, while hsCLDN-1 bound cCpE poorly, which agreed with its low binding capacity reported before (Fig. 1D, inset) (40). Additionally, we quantified cCpE binding to claudin-6, 17, and 19 because BLI measurements had not been reported for these subtypes. We measured K_{Ds} of 51.4, 27.0, and 27.5 nM for hsCLDN-6, 17, and 19, respectively (Fig. S2 and Table S2). In full, these results confirmed or established the cCpE receptor capacities of claudins, that homologous subtypes can bind cCpE with varied affinity owing to minute sequence alterations in key regions, and that the claudins we prepared were functional. This information was critical to benchmark against COP-1-binding studies.

Quantification of COP-1 binding to claudins

To determine COP-1s claudin-binding ability, we again performed single-point BLI analyses. We found that COP-1 bound all 13 claudins with <100 nM affinity that ranged from 59.0 to 99.6 nM with varied rates of association but similar rates of dissociation (Fig. 2A and Table 1). We then tested COP-1 binding to claudins in the presence of cCpE. This was done to determine whether the two proteins had overlapping binding sites and to determine whether cCpE binding could alter COP-1. Again, we found that COP-1 bound all claudins or claudin/cCpE complexes and generally that cCpE receptor claudins (claudin-3, 4, 6, 9, 17, and 19) yielded higher binding signal that nonreceptor claudins (claudin-1, 5, 15, and 18), owing to the larger masses of claudin/cCpE complexes vs. claudin alone detected by BLI (Fig. 2B). The cCpE alone did not bind COP-1. Analysis of the K_{Ds} revealed that COP-1's affinity for mmCLDN-3, hsCLDN-4, and hsCLDN-18.1 increased when cCpE was present, while for hsCLDN-17 and 19 it decreased—for all other claudins no significant change in COP-1 affinity occurred compared with cCpE alone (Table 1). COP-1 does not compete with cCpE and thus has a unique binding site yet is sensitive to claudin structural changes induced by cCpE.

To validate that COP-1 binds claudins specifically, we tested a homologous sFab discovered simultaneously with COP-1 called COP-2 for its ability to bind claudins (50). COP-2 is known to bind cCpE and hsCLDN-4/cCpE complexes but not hsCLDN-4 alone (50). Single-point BLI using COP-2 showed that it did not bind claudins in the absence of cCpE (Fig. S3A). However, when cCpE is added to claudins, COP-2 was found to bind to free cCpE in nonreceptor/cCpE mixtures or to cCpE in receptor/cCpE complexes (Fig. S3B). These experiments validated that COP-1 is unique in its claudin-binding ability due to sequence changes in its complementarity-determining regions compared with other sFabs that form nearly identical tertiary structures.

We next quantified COP-1 binding to all 10 claudin subtypes more extensively. We measured K_{Ds} of 61.3 nM for hsCLDN-1, 57.9 nM for hsCLDN-3, 70.6 nM for hsCLDN-4, 75.8 nM for hsCLDN-5, 59.5 nM for hsCLDN-6, 66.0 nM for hsCLDN-9, 59.0 nM for mmCLDN-15, 80.2 nM for hsCLDN-17, 92.4 nM for hsCLDN-18.1, 66.4 nM for hsCLDN-18.2, and 62.2 nM for hsCLDN-19 (Fig. 2C). This showed that COP-1 bound claudins with a range of 58–92 nM (Table 2). Using the dissociation rate (k_{off}), we calculated the half-life ($t_{1/2}$) of claudin/COP-1 complexes, which revealed that the $t_{1/2}$ of claudin/COP-1 complexes were between 8 and 13 min. We tested whether claudin/COP-1 complexes could be retained in solution using analytical size-exclusion chromatography (SEC) to validate this finding. By comparing the elution times of claudins alone (Fig. S4A) vs. claudins mixed with COP-1 and a sFab-specific nanobody (Fig. S4B), we found that COP-1s presence decreased average elution times from 5.6 to 5.1 min (Fig. S4C). This verified the formation of larger complexes at 5.1 min. COP-1 alone eluted at 7.2 min. These results suggested that the claudin/COP-1 complex is stable in vitro but is relatively short-lived, prompting us to determine whether COP-1 binds differently to claudins in membranes—a prerequisite for therapeutic applications.

COP-1 binds claudin-4 in membranes

Because claudins in detergent are not ideal proxies for how they may behave in vivo we tested whether COP-1 could bind claudins in membranes. Indication that it might came from previous findings that COP-1 bound hsCLDN-4 reconstituted in lipid nanoparticles called nanodiscs, which possesses a small lipid bilayer (51, 52). We reconstituted hsCLDN-4 in small unilamellar vesicles (SUVs) composed of the lipid diphytanoylphosphatidylcholine (DPhPC), which has been shown to produce functional claudin-4, and compared COP-1 binding to empty DPhPC SUVs (53). We found that empty SUVs gave a nonsensical and nonconcentration-dependent binding signal, whereas hsCLDN-4-loaded SUVs gave concentration-dependent binding signals with robust kinetic rates (Fig. 2D). We calculated a K_D and $t_{1/2}$ from the rates, which showed that COP-1 bound hsCLDN-4 in SUVs with 105.7 nM affinity and that the complex half-life approached 30 min (Table 2). The rates of COP-1 association (k_{on}) and dissociation (k_{off}) for hsCLDN-4 were >4-fold slower in SUVs compared with detergent. This finding showed that COP-1 binds claudins in membranes and that the complex is long-lived, piquing our interest to test its effect on claudins in epithelial cells.

COP-1 does not bind other tight junction membrane proteins

We next established whether COP-1 could bind other membrane proteins with extracellular domains found at tight junctions to rule out potential off-target effects in tissues. Occludin increases paracellular barrier function by driving the formation

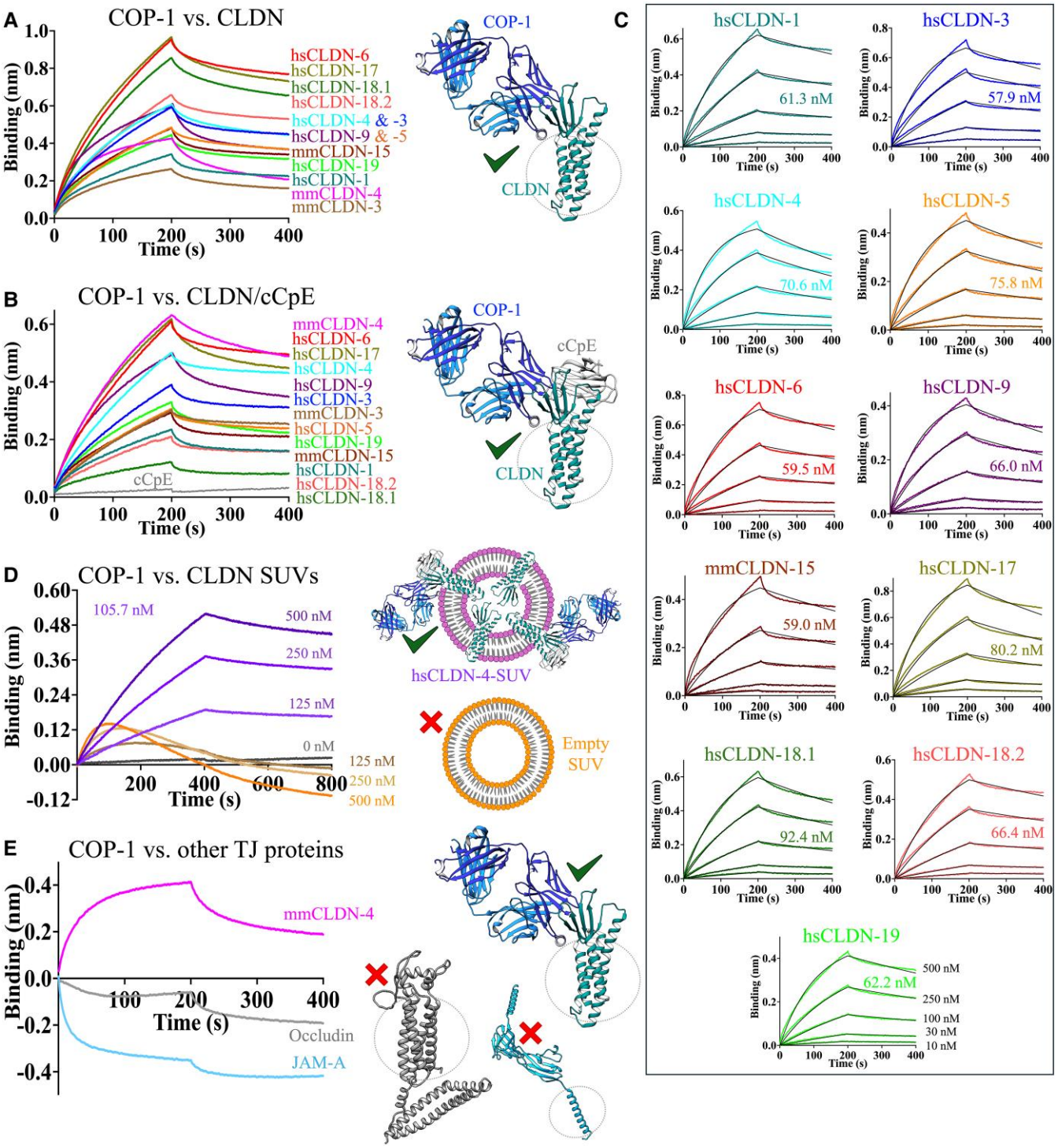

Fig. 2. COP-1 interactions with claudins and other tight junction proteins. A) Single-concentration point assessment of COP-1 binding to 13 claudin subtypes at 500 nM and B) single-concentration point analysis of COP-1 binding to 13 claudin subtypes in the presence of cCpE (250/250 nM). Table 1 shows the associated K_{Ds} values. C) Full multiconcentration point (0–500 nM) analyses of COP-1 binding to 11 representative claudin subtypes, and D) multiconcentration point (0–500 nM) analyses of COP-1 binding to SUVs loaded or unloaded with hsCLDN-4. Table 2 shows the associated kinetic rates and K_{Ds} values. E) Single-concentration point analysis of COP-1 binding to a control claudin (mmCLDN-4), human occludin, and JAM-A at 500 nM.

and stabilization of tight junction branching points (54, 55). Junctional adhesion molecule-A (JAM-A, also known as the F11 receptor) regulates membrane apposition and mediates intercellular signaling events at tight junctions while also serving as the large molecule barrier protein (56–58). We expressed and purified human occludin and JAM-A and found that they did not bind COP-1, which was verified by comparing to mmCLDN-4 (Fig. 2E). This result confirmed that COP-1 binds selectively to claudins and that any potential effects on barrier function observed in vivo would be a result of this selectivity and not binding to other extracellular domains of tight junction membrane proteins.

COP-1 binds distantly related members of the claudin/PMP22/EMP22/MP20 family

Because COP-1 bound all claudin subtypes that we assayed, we tested whether it could recognize distantly related members of the claudin/PMP22/EMP22/MP20 family (46, 47). Peripheral myelin protein 22 (PMP-22) and eye lens-specific protein 20 (MP-20) are 20–22 kDa claudin-like proteins that play roles in myelin synthesis and assembly and forming cell adhesive junctions in eye lenses and share 23.7 and 19.8% sequence identity with hsCLDN-4, respectively (59, 60). The urochordate *Ciona intestinalis* claudin-16 (ciCLDN-16) and Kune-kune from the invertebrate *Drosophila melanogaster* (dmKune) share 20.1 and 17.2% sequence identity to hsCLDN-4—dmKune is required for organization of septate junctions, the invertebrate equivalent of tight junctions (46, 61). Sequence alignments highlight this diversity and the regions where COP-1 may interact (Fig. S5). Structurally, these four proteins have four TMs, two ECS, and their predicted structures superimpose well onto hsCLDN-4, indicating they are indeed claudin-like (Fig. 3A) (62). A recent experimentally determined structure of MP20 further confirmed its fold (60). We expressed and purified human MP-20 and PMP-22, ciCLDN-16, and dmKune and found that COP-1 bound these claudin-like proteins (Fig. 3B). We calculated K_{Ds} of 2,778, 109.5, 115.1, and 238.1 nM for COP-1 binding to these four proteins, respectively (Table 2). To visualize the COP-1 interactions driving these affinity differences, we superimposed the models of MP-20, PMP-22, ciCLDN, and dmKune onto the hsCLDN-4 portion of PDB ID 8u4v. This revealed that residues in epitope 1 and the length of epitope 3 may explain the affinity differences that we measured (Fig. 3C). These results and modeling of COP-1 interaction interfaces confirmed that COP-1 binds the tertiary fold inherited among primary claudin/PMP22/EMP22/MP20 family members and affinity data show it can sense divergences between their sequence or structure.

Table 1. Single-point analysis of COP-1 binding to claudins.

Subtype	K_D (nM)	Complex	K_D (nM)
hsCLDN-1	76.3 ± 1.5	+cCpE	73.2 ± 1.5
hsCLDN-3	64.2 ± 1.1		58.5 ± 1.2
mmCLDN-3	90.5 ± 1.2		44.0 ± 0.9
hsCLDN-4	72.8 ± 0.9		42.4 ± 0.9
mmCLDN-4	99.6 ± 1.2		86.2 ± 0.8
hsCLDN-5	72.0 ± 1.1		65.5 ± 1.2
hsCLDN-6	59.0 ± 0.9		59.2 ± 1.0
hsCLDN-9	69.9 ± 1.2		74.8 ± 1.0
mmCLDN-15	63.3 ± 1.3		61.2 ± 1.4
hsCLDN-17	65.5 ± 0.9		86.4 ± 1.3
hsCLDN-18.1	83.4 ± 1.0		56.7 ± 1.4
hsCLDN-18.2	62.8 ± 1.1		55.6 ± 1.3
hsCLDN-19	62.4 ± 1.1		93.9 ± 1.4

COP-1 alters tight junction barrier permeability in an intestinal tissue model

We cultured Caco-2 cells and measured transepithelial electrical resistance (TEER) to evaluate the effect of COP-1 on tight junction barrier permeability. Confluent Caco-2 monolayers were treated at their apical and/or basolateral compartments with 500 nM COP-1 and various control proteins that included 500 nM cCpE, 200 nM CpE, and 500 nM COP-2. CpE is known to kill intestinal epithelial cells, while cCpE has been shown to modulate tight junction barrier permeability in tissue model monolayers (44, 63, 64). TEER was measured in transwell plates before the addition of test proteins and 24 h after treatment with a STX chopstick electrode and then on the same treated cells from the same wells using an Ussing chamber. TEER after treatment was compared with pretreatment for all proteins. Results with the STX electrode showed that COP-1-treated monolayers exhibited decreases in TEER of 19.6 and 37.3% after apical and basolateral delivery, respectively (Figs. 4A and S6A). The control protein cCpE decreased TEER by 12.7% when applied apically and 62.8% when applied basolaterally, consistent with previous findings (44, 65). Further, results of apical delivery of COP-2 and CpE showed that COP-2 had no effect, while CpE reduced TEER to ~0%, indicating obliteration of tight junction barriers after CpE-induced cytotoxicity (63). Ussing chamber TEER measurements agreed well with the STX electrode data and confirmed that COP-1 modulated tight junction barrier permeability (Fig. 4B). These results established that COP-1 modulates paracellular permeability in a manner and magnitude similar to cCpE.

We next determined whether Caco-2 tight junctions could be affected by COP-1 in a concentration-dependent manner, which was important to ascertain for therapeutic use. We found after COP-1 application to apical compartments that TEER decreased by 10.0% at 200 nM, 16.9% at 500 nM, 21.5% at 1,000 nM, 29.1% at 5,000 nM, and 71.0% at 9,000 nM as measured using a STX

Table 2. Full quantification of COP-1 binding to claudins.

Subtype	Mimetic	K_D (nM)	k_{on} (1/Ms)	k_{off} (1/s)	$t_{1/2}$ (min)	Epitope % ID
hsCLDN-1	Detergent	61.3 ± 0.5	$1.5 \times 10^4 \pm 0.7 \times 10^2$	$0.9 \times 10^{-3} \pm 5.4 \times 10^{-6}$	12.8	57
hsCLDN-3		57.9 ± 0.5	$2.1 \times 10^4 \pm 1.1 \times 10^2$	$1.2 \times 10^{-3} \pm 7.3 \times 10^{-6}$	9.6	91
hsCLDN-4		70.6 ± 0.4	$2.6 \times 10^4 \pm 1.2 \times 10^2$	$1.8 \times 10^{-3} \pm 7.1 \times 10^{-6}$	6.4	100
hsCLDN-5		75.8 ± 0.5	$1.9 \times 10^4 \pm 0.9 \times 10^2$	$1.5 \times 10^{-3} \pm 6.4 \times 10^{-6}$	7.7	76
hsCLDN-6		59.5 ± 0.4	$1.8 \times 10^4 \pm 0.9 \times 10^2$	$1.1 \times 10^{-3} \pm 6.0 \times 10^{-6}$	10.5	71
hsCLDN-9		66.0 ± 0.4	$2.2 \times 10^4 \pm 0.9 \times 10^2$	$1.5 \times 10^{-3} \pm 5.9 \times 10^{-6}$	7.7	67
mmCLDN-15		59.0 ± 0.5	$2.1 \times 10^4 \pm 1.2 \times 10^2$	$1.2 \times 10^{-3} \pm 8.2 \times 10^{-6}$	9.6	33
hsCLDN-17		80.2 ± 0.6	$1.9 \times 10^4 \pm 1.1 \times 10^2$	$1.5 \times 10^{-3} \pm 7.8 \times 10^{-6}$	7.7	29
hsCLDN-18.1		92.4 ± 0.5	$1.6 \times 10^4 \pm 0.7 \times 10^2$	$1.4 \times 10^{-3} \pm 4.9 \times 10^{-6}$	8.3	33
hsCLDN-18.2		66.4 ± 0.5	$1.3 \times 10^4 \pm 0.7 \times 10^2$	$0.9 \times 10^{-3} \pm 5.2 \times 10^{-6}$	12.8	19
hsCLDN-19		62.2 ± 0.4	$1.7 \times 10^4 \pm 0.7 \times 10^2$	$1.1 \times 10^{-3} \pm 5.3 \times 10^{-6}$	10.5	57
hsCLDN-4	SUV	105.7 ± 0.3	$0.4 \times 10^4 \pm 0.1 \times 10^2$	$0.4 \times 10^{-3} \pm 0.7 \times 10^{-6}$	28.9	100
hsMP-20	Detergent	2,778 ± 242.8	$4.0 \times 10^4 \pm 0.3 \times 10^2$	$1.1 \times 10^{-1} \pm 1.3 \times 10^{-3}$	0.1	N/A
hsPMP-22		109.5 ± 0.8	$1.8 \times 10^4 \pm 1.0 \times 10^2$	$2.0 \times 10^{-3} \pm 9.4 \times 10^{-6}$	5.8	N/A
ciCLDN-16		115.1 ± 1.1	$2.7 \times 10^4 \pm 1.7 \times 10^2$	$3.1 \times 10^{-3} \pm 21.0 \times 10^{-6}$	3.8	N/A
dmKune		238.1 ± 2.9	$1.8 \times 10^4 \pm 1.8 \times 10^2$	$4.4 \times 10^{-3} \pm 30.6 \times 10^{-6}$	2.7	N/A

N/A, not analyzed.

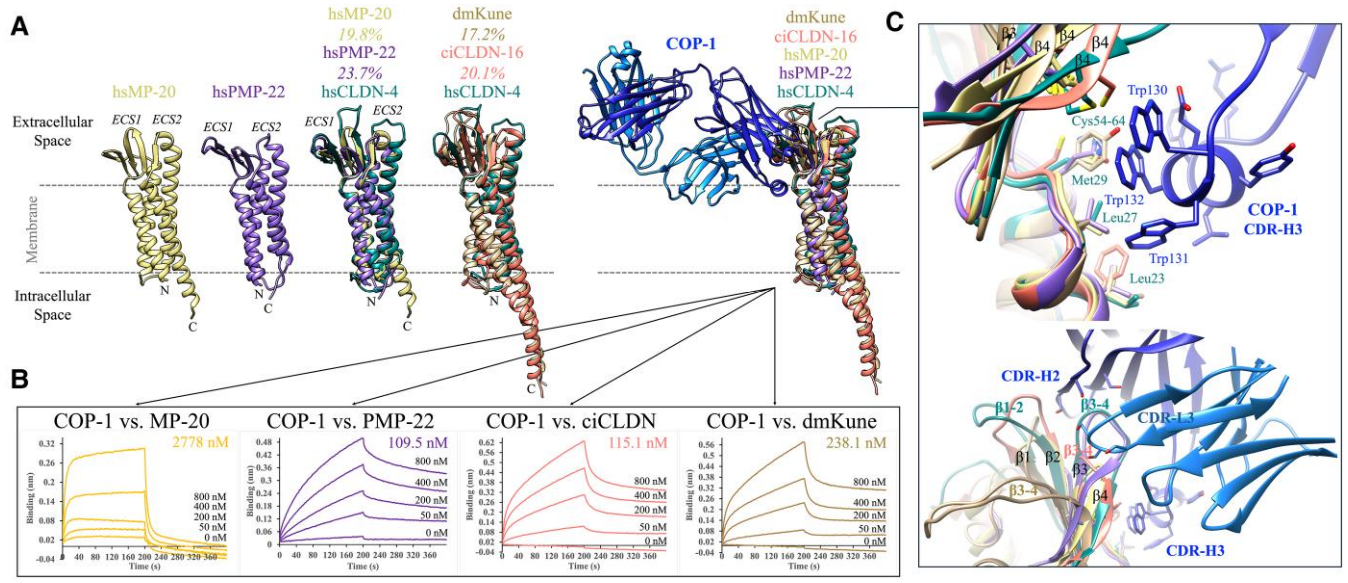

Fig. 3. COP-1 interactions with distantly related claudin/PMP22/EMP22/MP20 family members. A) Models from AlphaFold of hsMP-20 (yellow), hsPMP-22 (purple), ciCLDN-16 (salmon), and dmKune (brown) were superimposed on the experimental structure of hsCLDN-4 (teal). The cryo-EM structure of COP-1 bound to hsCLDN-4/cCpE (PDB ID 8u4v) shows a potentially shared mode of COP-1 binding to these four proteins. B) Full multiconcentration point (0–800 nM) analyses of COP-1 binding to claudin homologs. Colors of binding traces match structures in A). C) Zoom-in of epitopes 1 and 3 on claudins and claudin-like proteins where COP-1 likely binds based on BLI results and cryo-EM structure PDB ID 8u4v.

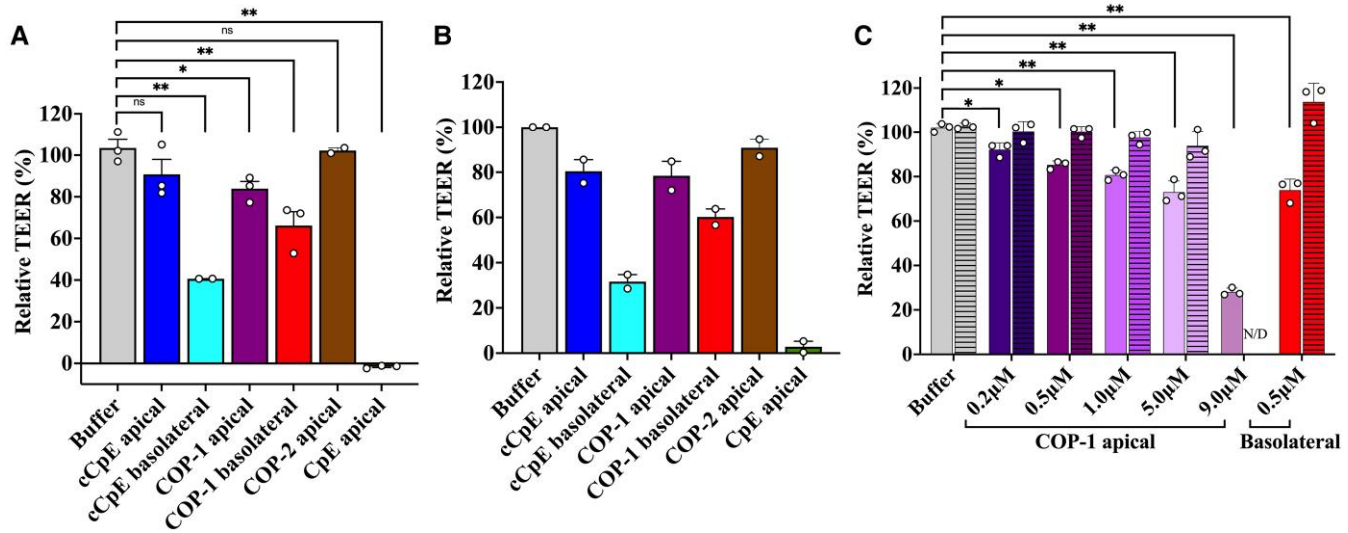

Fig. 4. Effect of COP-1 on tight junction barrier integrity in a model for intestinal epithelium. A) Plot of relative TEER measurements using an STX electrode after delivery of various proteins to the apical or basolateral compartments of Caco-2 monolayers. Proteins include cCpE, COP-1, COP-2, and CpE. TEER was measured $n = 2$ for cCpE basolateral and COP-2 apical treatments and measured $n = 3$ for buffer, COP-1 apical and basolateral, cCpE, and CpE apical treatments. B) Plot of relative TEER measurements using an Ussing chamber from the same monolayers used in A). TEER was measured $n = 2$ for all concentrations. C) COP-1 concentration-dependent decrease in TEER. A concentration range (0–9,000 nM) of COP-1 was added to apical compartments and single concentration (500 nM) added to basolateral compartments of Caco-2 cells, and TEER was measured using a STX electrode, $n = 3$. The recovery of barrier function was measured after removal of COP-1. Solid bars represent the data from 24 h, while patterned bars represent the data from 48 h (that is 24 h after COP-1-containing media are exchanged with fresh medium), $n = 3$. The 48-h timepoint for 9 μM COP-1 apical measurement was not determined (N/D). There is no significant difference between the cells before treatment and after recovery. All data are represented as mean ± SEM of two or three independent measurements. *$P < 0.05$ and **$P < 0.001$ in TEER from treated cells compared with buffer alone.

electrode after 24 h treatment compared with buffer alone (Figs. 4C and S6B). We then determined whether tight junction permeability was reversible by removing COP-1 containing medium, exchanging it for fresh medium, and then measuring TEER 24 h after exchange. We found that TEER increased back to pretreatment levels for monolayers treated with <1,000 nM COP-1 but not for monolayers treated with >1,000 nM COP-1 (Fig. 4C). We also found in monolayers treated with 500 nM COP-1 at their apical or basolateral compartments that TEER recovered more completely in basolaterally treated cells. Altogether, these results indicated that COP-1 increases paracellular permeability of a model epithelium in a concentration-dependent and reversible manner and that this modulating effect may be prolonged upon apical delivery.

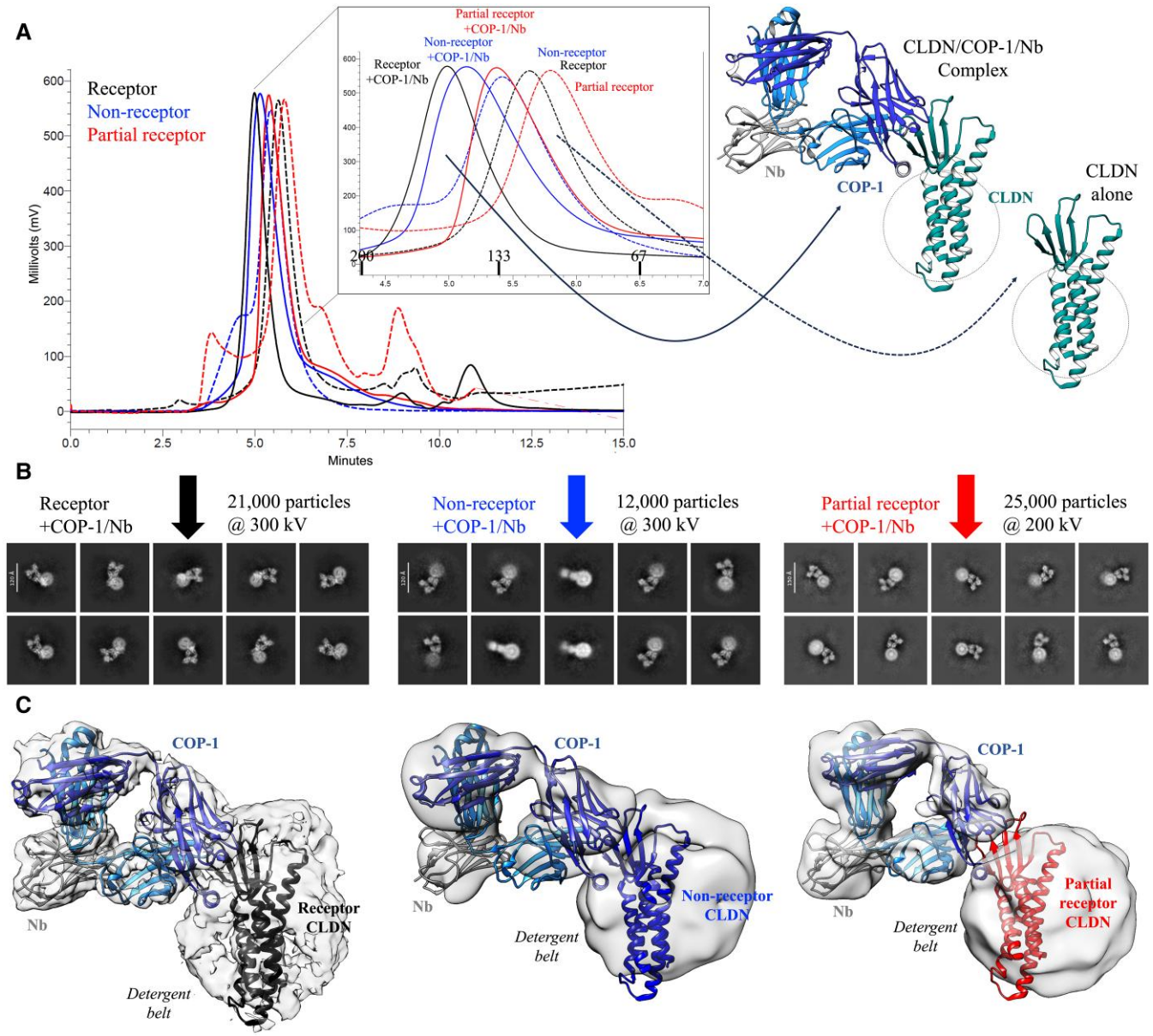

Fig. 5. Structural basis of COP-1 binding to claudins. A) SEC chromatograms showing the elution times of claudins alone (dashed lines) vs. claudin/COP-1/Nb complexes (solid lines). Structural models of the expected complexes are shown based on PDB ID 8u4v where claudins and COP-1 are depicted as cartoons. B) 2D classifications and C) 3D reconstructions from cryo-EM of claudin/COP-1/Nb complexes from the three cCpE receptor classes (receptors, black; nonreceptors, blue; partial receptors, red). Note that the quality of 2D classes and final maps varies and that all three maps in C) have been contoured to a level (0.09) optimized for receptor claudins to highlight differences in quality.

Structural basis of COP-1 binding to claudins

Lastly, we attempted to elucidate the structural basis of COP-1's claudin-binding ability and to assess whether COP-1 could enable structure determination of claudins. Because claudins are dynamic and low molecular–weight proteins, they are recalcitrant to structural determination by cryogenic electron microscopy (cryo-EM). The sFabs COP-1 and 2 were developed to act as fiducial marks to enable structures by cryo-EM (32, 50). We incubated COP-1 and an anti-sFab nanobody (Nb) with cCpE and claudins from each of the three cCpE receptor classes and isolated claudin/COP-1/Nb complexes (Fig. 5A). The complexes were vitrified on grids and imaged using 200 or 300 kV microscopes. Processing of the cryo-EM data yielded 2D classifications representative of claudin/COP-1/Nb complexes where the sFab/Nb is observed bound to a circular mass (Fig. 5B). Experimental limitations, owing to complex dissociation or orientation bias, yielded moderate-resolution (4–9 Å) maps and 3D reconstructions of variable quality where COP-1/Nb were well resolved but the claudins were not (Figs. 5C and S7). The detergent belt encasing claudins dominates the signal and masks the claudin, making them largely unresolvable in the maps. Because of the high confidence we had in COP-1/Nb placement, we modeled the structure of hsCLDN-4/COP-1/Nb bound to cCpE (PDB ID: 8u4v) into the maps, which showed that COP-1 binds all claudins tested in an identical manner (Fig. 5C). Although COP-1 was not able to yield high resolution structures of claudins by cryo-EM, these results verified our biochemical and biophysical findings and provided validating structural information for COP-1s claudin-binding mechanism.

Discussion

We developed sFabs against cCpE and hsCLDN-4 to enable structure determination by cryo-EM (32, 50). Upon structural and biophysical characterization of the hsCLDN-4-binding sFab, COP-1, we discovered cross-reactivity with homologous claudins and that the epitopes that COP-1 used to bind hsCLDN-4 had sequence identity across the claudin family (Fig. 1C). This initially allowed us to predict that COP-1 could also bind claudin-3, 5, 6, and 9 (32). Here, we isolated 13 claudins representing 10 subtypes and tested COP-1s claudin-binding ability, benchmarking it against the well-characterized claudin-binding protein cCpE. Applying our findings, we can classify the 13 claudins tested into three categories based on their affinity for cCpE, which include receptors (mmCLDN-3, hsCLDN-4, mmCLDN-4, hsCLDN-9), partial receptors (hsCLDN-3, hsCLDN-6, hsCLDN-17, and hsCLDN-19), and nonreceptors (hsCLDN-1, hsCLDN-5, mmCLDN-15, and hsCLDN-18.1 and 18.2). This classification stems from the ability of claudins to bind cCpE at 500 nM, which is slightly above the pathophysiological concentration maximum of 350 nM (43). Coupled with the sequence diversity within claudins that define classic and nonclassic subtypes, cCpE receptor capacity becomes a useful characteristic to interpret the structure and function of claudins. In this study, it becomes important to benchmark COP-1 function and potential application against cCpE. Additionally, and more importantly, we establish here that COP-1 is a high-affinity (<100 nM) and pan-claudin-binding molecule with a unique binding mode and binding site that encompasses the TM and extracellular domains of claudins, which is distinct from cCpE's. In full, our binding analyses demonstrate that COP-1 binds uniquely and more broadly to claudins compared with cCpE.

Our biophysical results show that COP-1 binding to claudins is not altered dramatically in the presence of cCpE, indicating that its binding epitopes are structurally similar when bound or unbound to cCpE (Table 1). This finding makes sense because cCpE binds the palm region of the claudin hand, while COP-1 binds epitopes that reside on the back of the claudin hand (Fig. 2B). This led us to speculate that COP-1 could bind claudins in any environment if these epitopes are accessible. We validated this theory by showing that COP-1 binds hsCLDN-4 in SUVs (Fig. 2D). Although we did not assess whether claudins are oligomeric in SUVs or whether hsCLDN-4-SUVs interact in trans, this finding is significant because it demonstrates that claudin structure in detergents approximates those in membranes and that in vitro results may translate in vivo. Further, we provide evidence that COP-1 selectively binds claudins and other members of the claudin/PMP22/EMP22/MP20/voltage-gated calcium channel γ subunit (pfam00822) superfamily with our data that show COP-1 binds MP-20 and PMP-22 (Fig. 3) but not occludin or JAM-A, two other tight junction membrane proteins that are structurally unique from claudins but which also have TM and extracellular domains (Fig. 2E) (46). Notably, COP-1 distinguishes claudins from occludin, which has a similar four TM domain architecture but larger ECS (54). Our findings verify that COP-1 is a pan-claudin-binding molecule and that claudins, PMP-22, and MP-20 are structurally homologous. We hypothesize that COP-1 may be used to modulate the plethora of cellular functions at cell/cell contacts and beyond in invertebrates and vertebrates that other claudin/PMP22/EMP22/MP20 family members perform in specific ways—expanding its applicability.

We previously used a cryo-EM structure to pinpoint the three COP-1-binding epitopes on claudins and concluded that epitope 1 was the primary determinant (32). We can now refine these conclusions with data from seven more subtypes and three claudin-like proteins. It is apparent that COP-1 broadly recognizes the claudin fold due to the large sequence divergences in tested claudin and claudin-like proteins, which suggests that individual side chains play a smaller role in COP-1 binding than tertiary structure. Experiment and structural predictions show that the length and structure of TM1, the turn connecting it to β-strand 1 (epitope 1), as well as the five-stranded β-sheet structure of ECS (epitopes 2 and 3), are conserved in all proteins tested (Fig. 3A). This conserved global extracellular structure explains why COP-1 binds claudins with a tight range of 58–92 nM affinity (Fig. 2C) and why it also binds claudin-like proteins (Fig. 3B), albeit with lower affinities. The key claudin residues for COP-1 binding based on sequence homology and mutant data appear to be Leu23, Leu27, and Met29 (hsCLDN-4 numbering) in epitope 1—where long hydrophobic side chains at these positions are mostly conserved (Figs. 3C and S1). For claudin-like proteins, which vary in epitope 1 sequence, we suspect that measured differences in affinity are the result of changes to epitope 3 that alter the length of the loop connecting β3 to β4 (Figs. 3C and S5). All claudins and claudin-like proteins have a conserved disulfide bond in β3–4 that defines the length of the β3–4 loop. The length of this loop in human and mouse claudins does not fluctuate by more than one amino acid, which explains their tight affinity ranges (Fig. S1). However, while PMP-22's β3–4 loop is as long as a claudin (10 vs. 9 residues), ciCLDN's and MP-20's are shorter (five and four residues) and dmKune's is longer (17 residues) (Figs. 3C and S5). Because the β3–4 loop binds between COP-1s H and L chains, it is a key element of COP-1 binding. Our data that show COP-1 binds PMP-22 > ciCLDN > dmKune >> MP-20 best to worst (Fig. 3B) demonstrate that the length of the β3–4 loop plays a key role in COP-1 binding, as loops too short or too long greatly affect affinity, likely by preventing the H and L chains of COP-1 from clamping onto it. In full, our extended data show that epitopes 1 and 3 on claudins direct COP-1 binding and that COP-1 affinity can be altered with targeted substitutions or alterations in length within these key regions.

COP-1s claudin-specific and extracellular domain binding, like cCpE, makes it an ideal molecule to alter tight junction barrier function, so we tested this in a model intestinal epithelium. COP-1 disrupts tight junction barriers in Caco-2 monolayers after both apical and basolateral application and this disruption is reversible (Fig. 4). Apical delivery of COP-1 also decreases TEER in a concentration-dependent manner and once removed, tight junction barrier function is restored, although the magnitude of recovery is also concentration-dependent and potentially time-dependent. Barrier recovery appears more complete if COP-1 is delivered to basolateral vs. apical compartments. Compared with the known tight junction disruptor cCpE (44, 45), COP-1 decreases barrier integrity equivalently when applied apically, whereas basolateral treatment shows cCpE is more effective. In full, our data suggest that COP-1 and cCpE open paracellular barriers to similar degrees using similar mechanisms—the details of which can be elucidated by considering how claudins integrate into tight junctions and the amount of cCpE receptor claudins a given tissue contains.

Van Itallie et al. (66) showed that new claudins, those yet to polymerize, are integrated into tight junction strands through basolateral pools to keep apical barriers intact. Old claudins are subsequently removed from apical strands in unknown oligomeric states to then perform other functions or to be degraded. Caco-2 cells express claudin-1, 2, 3, 4, 7, and 15 (65, 67). These represent classic and nonclassic and all three classes of cCpE receptor (Fig. 1B and D). Basolateral delivery of cCpE will readily bind non-polymerized claudin-3 and 4 and prevent their integration into tight junction strands, affecting barrier function. This "sequestering" mechanism described by Sonoda et al. (44) is based on their

finding that basolateral but not apical delivery of cCpE to MDCK monolayers decreased TEER posits that cCpE disrupts the equilibrium between nonpolymerized and polymerized claudins. The decreases to TEER in Caco-2 monolayers we find after basolateral delivery of both cCpE and COP-1 agree with a sequestering mechanism—with the difference being that cCpE binds only receptor claudins, whereas COP-1 binds all claudins—yet both likely sequester claudins from integration into tight junctions. We speculate that the greater effect on TEER by basolateral cCpE can be explained by several factors. First, intestinal epithelium and Caco-2 cells are rich in cCpE receptors, so cCpE can have a greater impact on barrier function in such tissues (65, 67). Second, cCpEs higher affinity binding and longer complex half-life for claudins would sequester them better and longer from polymerizing compared with COP-1 (Table S2). Third, cCpE binding is known to alter the structures of claudins, while COP-1 adapts to their structures (32, 36, 37, 39, 68). And fourth, the COP-1 epitope may not be as accessible in polymerized or nonpolymerized claudins as cCpE-binding surface—more on this to follow. These factors, coupled with the integration of claudins into tight junctions from basolateral pools, explain why cCpE is a better modulator of barrier function than COP-1 when applied basolaterally.

Apical delivery of cCpE and COP-1 decreased TEER equally, while higher amounts of COP-1 decreased TEER further in concentration-dependent and reversible ways (Fig. 4) (63). These findings suggest that cCpE and COP-1 bind polymerized claudins within tight junctions. In the more developed apical tight junctions, old claudins are removed from active strands but new ones are not synthesized from there (66). Thus, cCpE or COP-1 binding to nonpolymerized apical claudins would not alter the polymerized/nonpolymerized equilibrium to affect barrier integrity. This idea agrees with our results that apical treatments decrease TEER less that basolateral application and that TEER recovers more completely after basolateral treatment of COP-1 compared with apical. To affect the barrier integrity of epithelium, cCpE and COP-1 must bind polymerized claudins and subsequently alter tight junction structure. This is a challenge because unlike nonpolymerized claudins, polymerized claudins are proposed to associate in distinct ways that may shield cCpE and COP-1-binding surfaces. Our results suggest that cCpEs and COP-1s binding epitopes are at least partially accessible in claudin-polymerized tight junctions because these proteins decrease TEER when applied apically. These findings provide further evidence that COP-1 may be as potent of a tight junction modulator as cCpE but that it could have enhanced applicability as it does not rely on specific receptors and could thus open tight junctions as cCpE does but in nontissue-specific ways.

Shrestha et al. (63) found that 285 nM cCpE delivered apically to Caco-2 cells decreased TEER by 50% overnight, while we found that 500 nM COP-1 decreased TEER by ~22%. This suggests that although both proteins target claudins in tight junctions, that like basolateral treatment, cCpE is more effective. Again, this could be because Caco-2 cells are richer in receptor claudins and cCpE is better at binding and altering these subtypes than COP-1 is at doing so generally; or, that there are differences in subtype composition in apical vs. basolateral strands, as has been suggested and shown (43, 69); or, that the COP-1 epitope is not as accessible as cCpE-binding surface in polymerized claudins. To understand how cCpE, COP-1, or any molecule alters claudin structure to affect apical tight junction barriers requires structures of polymerized claudins. Unfortunately, no experimental structures exist. However, using models of polymerized claudins we find that cCpE- and COP-1-binding surfaces may indeed be differentially accessible (8, 48, 70–72). In straight lateral assemblies, both cCpE and COP-1 surfaces are accessible (Fig. S8A) (48); in face-to-face dimers (X-1), only cCpEs surface is accessible (Fig. S8B) (71); in an alternate dimer (Cis-1), cCpEs surface is accessible but COP-1s is partially occluded (Fig. S8C) (70); and in a yet verified dimer that we generated, both protein's surfaces are accessible (Fig. S8D). These models of polymerized claudins suggest that cCpE-binding surface is available in more claudin polymers than COP-1s. We hypothesize that unlike cCpE, COP-1 could be used to elucidate the organization of polymerized claudins in different tissues as it may only bind effectively to distinct claudin polymers. Further validation of these models of polymeric claudins is needed to test this idea and to develop better claudin-binding molecules.

In sum, COP-1 is a pan-claudin-binding molecule capable of reversibly modulating paracellular permeability in model intestinal epithelium through targeted disruption of tight junctions. COP-1 has the potential for "tunability" because apical delivery directly insults tight junctions and recovers slower than basolateral delivery, which is more dynamic as the site of claudin synthesis and integration. Synthetic COP-1 is nearly as effective at opening tight junction barriers in intestinal tissues as a highly evolved, natural, and subtype-selective tight junction modulator, cCpE. COP-1s pan-claudin-binding ability may enable it to outperform cCpE in barrier disruption of more diverse epithelia or endothelia. Explicitly, we surmise that COP-1s insult to tight junction barrier integrity will be greater than cCpEs in tissues lacking cCpE receptor claudins but rich in other subtypes because both modulators have overlapping mechanisms of barrier disruption but unique modes of binding. Thus, for modulating paracellular permeability, COP-1 may have increased potency, while its claudin specificity yields low off-target effects. As is, or with increased development, COP-1 may serve a wide range of translational applications that include modulation of tight junctions, drug delivery through paracellular spaces, detection of claudin-rich cancers, or inhibition of inflammatory or oncogenic pathways.

Materials and methods

Sequence analysis of claudins

All claudin sequences were obtained from UniProt database (73). We performed multiple sequence alignment and phylogenetic analysis with T-coffee on the EMBL-EBI webserver (74, 75). The aligned claudin sequences were viewed and colored according to sequence identity in Jalview (76). The secondary structural elements, as marked on the sequence alignment, were mapped out based on human claudin-4 structure (PDB ID: 7kp4).

Protein expression and purification

All claudins (hsCLDNs, mmCLDNs, ciCLDN, dmKune) and cCpE were expressed and purified as previously described (32, 39, 40). All proteins contained a terminal polyhistidine tag with thrombin protease cleavage site. Proteins were expressed in insect cells, purified by immobilized metal affinity chromatography, and then released from NiNTA resin after thrombin digestion. Protein purity and homogeneity were verified by SDS–PAGE and SEC, and then, concentrated stocks (1 mg/mL) were snap frozen in liquid N and stored at −80 °C until use. MP-20 and PMP-22 were purified as previously described (60, 77, 78). For PMP-22, the post-NiNTA protein was polished further using anti-FLAG M2 resin (Sigma). Both proteins were snap frozen in liquid N, stored at −80 °C, and then sent to the Vecchio lab for analysis. After rapid thawing at 37 °C, they were placed on ice and then used for binding studies.

COP-1 and 2 with and without a C-terminal histidine tag were expressed in BL21 (DE3) cells using pRH2.2 plasmid encoding the gene for the protein as previously described (32, 50). Briefly, cells transformed with COP plasmid were used to inoculate a 1-L culture in TB media containing 100 µg/mL ampicillin, then grown to an OD of 0.8, and induced with 1 mM IPTG. Cells were harvested by centrifugation and lysed by sonication, and then, lysate was incubated at 65 °C for 30 min and rapidly chilled on ice for 15 min. Lysate was centrifuged at 8,200×*g*, filtered, then loaded onto a protein L column (Cytiva) in 20 mM Tris pH 7.4, 100 mM NaCl, and 1% glycerol. For COP-1, 0.01% *n*-dodecyl-β-D-maltoside (DDM, Anatrace) was added throughout the prep. COPs were eluted then dialyzed in BLI buffer (20 mM Tris pH 7.4, 100 mM NaCl, 1% glycerol, 0.03% DDM). COP-1 was concentrated to 1 mg/mL, snap frozen in liquid N, and stored at −80 °C until use.

Reconstitution of hsCLDN-4 in SUVs

Thirty-five milligrams of DPhPC were dried under nitrogen gas for 90 min and then rehydrated in 2 mL of SUV buffer (25 mM HEPES pH 7.4, 150 mM NaCl, and 0.5 mM TCEP). The solution was tip sonicated for 4 min to make SUVs and then filtered 10× through a 0.2-µm syringe filter (Pall). One hundred and forty microliters of SUV buffer with 1% *n*-octyl-β-D-glucoside (OG) were used to make empty SUVs, while 70 µL of 2 mg/mL hsCLDN-4 in DDM was mixed with 70 µL of SUV buffer with 2% OG to make hsCLDN-4-SUVs. To 140 µL of both solutions, 340 µg of DPhPC SUVs and SUV buffer was added to 175 µL and incubated on the bench for 30 min. This solution was diluted 4-fold, then placed in 3-mL Slide-a-lyzer 10 kDa MWCO cassette (Pierce), and dialyzed against 250 mL of SUV buffer in the presence of 2 g SM2-biobeads (Bio-Rad) overnight at 4 °C. One hundred and forty micrograms of hsCLDN-4 in 875 µL yielded 0.16 mg/mL (6.95 µM). This stock was used for BLI analyses, although only half of hsCLDN-4s may be oriented outside-out.

Biolayer interferometry

BLI was performed on an Octet R8 (Sartorius) at 25 °C in 96-well black flat bottom plates (Greiner) using an acquisition rate of 5 Hz averaged by 20. Histidine-tagged proteins (500 nM cCpE, 100 nM COP-1, or 100 nM COP-2) in BLI buffer were immobilized on Ni-NTA Dip and Read biosensors, and then, a kinetic experiment was performed that consisted of baseline (100 s), association (200–300 s), and dissociation (200–300 s) steps. Claudins, claudin-like proteins, (0–2,000 nM), or claudin/cCpE complexes (250/250 nM) in BLI buffer were present in association wells for analyses. For MP-20, histidine-tagged MP-20 (300 nM) was immobilized on Ni-NTA sensors then dipped in wells containing untagged COP-1 (0–800 nM) in BLI buffer. For binding of COP-1 to SUVs, SUV buffer was used and 100 nM COP-1 or 500 nM cCpE was tested against hsCLDN-4-SUVs (0–500 nM). The binding of hsCLDN-4-SUVs to immobilized cCpE verified that some claudin ECSs were outside-out facing. An equal volume of empty SUVS were used, as these had no Abs_{280nm} due to not being loaded with a protein. All binding measurements were fit to a 1:1 binding model using BLitz Pro 1.3 software, and then, the kinetic data and fits were exported is.csv format and replotted using GraphPad Prism version 10.0.3 or Microsoft Excel version 16.92.

Size-exclusion chromatography

To assess COP-1 binding to claudins using SEC, 100 to 250 µg of claudin was added to 1 M equivalent of COP-1 and incubated at 4 °C overnight. A 1.2 M excess of anti-sFab nanobody to COP-1 was added and incubated for 2 h at 4 °C. Solutions were 0.2 µm filtered and loaded onto a Superdex 200 increase (5/150) gl (Cytiva) column equilibrated in BLI buffer. The formation of complexes between claudin and COP-1/Nb was assessed by comparing elution times of claudin alone to claudin/COP-1/Nb.

Transepithelial electrical resistance

Human colorectal adenocarcinoma cells (Caco-2) cells, obtained from the American Biological Culture Association, were a kind gift from the Duffey Lab, Department of Physiology and Biophysics, University of Buffalo. Cells were grown and maintained in DMEM, high glucose, GlutamMAX supplement, pyruvate (Gibco) supplemented with 10% fetal bovine serum, 1× MEM nonessential amino acid solution (Sigma Aldrich), and 1% penicillin–streptomycin. Caco-2 cells were seeded onto transwell plates (12 mm pore, 0.4 µm pore polycarbonate membrane, Corning Costar) and grown to confluency for at least 14 days at 37 °C with 5% CO_2 with a change of media every 48 h. For the assay, confluent monolayers were treated with medium (no serum) containing 500 nM cCpE, 500 nM COP-1, 500 nM COP-2, 200 nM CpE, or buffer for 24 h. cCpE and COP-1 were added to the apical and basolateral compartments separately, while CpE, COP-2, and buffer only were added to the apical compartment only. All proteins were dialyzed in Tris-buffered saline and 0.2 µm filtered before use. TEER was measured using the Millicell-ERS (Electrical Resistance System) epithelial volt-ohmmeter (Millipore Sigma) and STX2 chopstick electrode (WPI) and normalized by the surface area of the monolayer. TEER values were calculated using the following equation: (Cell resistance − Blank resistance) (ohms) × membrane surface area (cm^2). TEER values were obtained before treatment with proteins and after overnight incubation with proteins. For the COP-1 concentration-dependent assay, 200 to 9,000 nM COP-1 was added to the apical compartment of Caco-2 monolayers and TEER was recorded as described above using the STX2 chopstick electrode. After measuring, media containing COP-1 were removed from the monolayers and replaced with fresh media and then TEER was measured again after 24 h.

TEER measurements from cell cultures treated as above were also measured using a modified Ussing chamber (Physiologic Instruments). After treatment with test proteins, Caco-2 monolayers were removed from the transwell plate, mounted in the Ussing chamber, and bathed in a ringer pH 7.4 buffer solution containing 119 mM NaCl, 21 mM $NaHCO_3$, 2.4 mM K_2HPO_4, 0.6 mM KH_2PO_4, 1.2 mM $MgCl_2$, 1.2 mM $CaCl_2$, and 10 mM glucose, at 37 °C in the presence of 5% CO_2. Basal TEER readings of each monolayer in the ringer solution were then recorded for ∼2 min.

Cryo-EM

Claudins purified as described above were exchanged from DDM to 2,2-didecylpropane-1,3-bis-β-D-maltopyranoside (LMNG) detergent via a PD-10 column (Bio-Rad). COP-1 was added in 1.4 moles excess to claudins, and then, 1.4 moles excess Nb to COP-1 were mixed and incubated at 4 °C for 1 h. To keep COP-1 bound to claudins, cCpE was added at 1.4 moles excess to claudin as affinity data suggested cCpE's presence can improve COP-1 binding (Table 1). Complexes were concentrated, filtered, and injected onto a Superdex 200 increase (5/150) gl (Cytiva) column equilibrated in 20 mM HEPES pH 7.4, 100 mM NaCl, and 0.003% LMNG. Peak fractions were pooled and concentrated to 4 mg/mL. The complex (3.5 µL) was then applied to UltrAuFoil 1.2/1.3 300 mesh (Quantifoil) grids that were glow-discharged for 60 s at 15 mA using a Pelco easiGlow (Ted Pella Inc.). Grids were blotted for 5 s and

then plunge frozen into liquid ethane cooled by liquid nitrogen using an EM GP2 (Leica) plunge freezer at 4 °C and 100% humidity. Grids were stored in liquid nitrogen and then imaged using either a 200 or 300 kV cryo-TEM.

For the receptor COP-1/Nb complex, data collection was performed on a Titan Krios G3i (ThermoFisher) equipped with a Gatan K3 direct electron detector and BioQuantum GIF at the University of Chicago Advanced Electron Microscopy Core Facility (RRID: SCR_019198). 6,774 movies were collected using EPU (ThermoFisher) in CDS mode at 105,000×*g* magnification with a superresolution pixel size of 0.827 Å, a physical pixel size of 1.65 Å, and a defocus range of −0.9 to −2.1 μm with a total dose of 70 electrons/Å^2. For the nonreceptor COP-1/Nb complex, data collection was performed at the Pacific Northwest Cryo-EM Center (PNCC) on a Titan Krios G3i (ThermoFisher) equipped with a Gatan K3 direct electron detector and BioContinuum HD GIF. A total of 4,801 movies were collected using SerialEM in counting mode at 130,000×*g* magnification with a physical pixel size of 0.649 Å, a superresolution pixel size of 0.324 Å, and a defocus range of −0.8 to −2.4 μm with a total dose of 50 electrons/Å^2. For the partial receptor COP-1/Nb complex, data collection was performed at the Hauptman–Woodward Medical Research Institute (HWI) on a Glacios 2 (ThermoFisher) equipped with a Falcon 4i direct electron detector. A total of 1,019 movies were collected using EPU (ThermoFisher) at 120,000×*g* magnification with a physical pixel size of 0.884 Å and a defocus range of −0.4 to −1.8 μm with a total dose of 50 electrons/Å^2.

Micrograph and particle processing were performed in CryoSPARC (79). After patch-motion correction and patch-CTF correction of micrographs, blob-based particle picking followed by template-based picking yielded particles of claudin/COP-1/Nb complexes. Note that for all three receptor classes, particles from initial 2D classifications were chosen that did not contain cCpE. These particles were then subjected to subsequent rounds of 2D classifications, followed by ab initio 3D reconstruction and nonuniform refinement to yield the final maps (Fig. S7). Using the claudin/COP-1/Nb portion of PDB ID 8u4v, Chimera was used to fit the model into each map (80). No further model building or refinement of structures was conducted as the maps were not high resolution enough to visualize claudins.

Statistical analysis

Values from independent experiments are shown as mean ± SEM. Statistical analysis for relative TEER measurements was performed by one-way ANOVA and Dunnett's multiple comparison test. For statistical analysis comparing different protein treatments before and after treatment, paired Student's t test analysis was used for the two-group comparison using GraphPad Prism, version 10 (GraphPad, San Diego, CA, USA). Differences were considered significant when the *P*-value was <0.05.

Acknowledgments

The authors are grateful to the University of Chicago Advanced Electron Microscopy Core Facility (RRID:SCR_019198), to Craig Yoshioka, Claudia López, and Sean Mulligan at PNCC, and to Devrim Acehan and Katherine Spoth at HWI Cryo-EM Center for cryo-EM access.

Supplementary Material

Supplementary material is available at *PNAS Nexus* online.

Funding

Research reported in this publication was supported by the National Institute of General Medical Sciences of the National Institutes of Health under award numbers: R35GM138368 (A.J.V.), P41GM136508 (T.G.), R01NS095989 (C.R.S.), and R01GM117372 (A.A.K.). The content is solely the responsibility of the authors and does not necessarily represent the official views of the National Institutes of Health. The Gonen laboratory (T.G.) was supported by funds from the Howard Hughes Medical Institute. The Sanders laboratory (C.R.S.) acknowledges funding from the Charcot-Marie-Tooth Research Foundation award 2023-0049. A portion of this research was supported by NIH grant U24GM129547 and performed at the PNCC at OHSU and accessed through EMSL (grid.436923.9), a DOE Office of Science User Facility sponsored by the Office of Biological and Environmental Research.

Author Contributions

A.J.V. designed research. C.P.O., A.J.V., A.M.M., X.L., S.K., J.C., Y.N.R., and M.C.G. performed research. M.d.l.A., C.R.S., T.G., A.A.K., and M.E.D. contributed new reagents and analytical tools. C.P.O. and A.J.V. analyzed the data and wrote the paper.

Preprints

A previous version of this manuscript was posted as a preprint that can be viewed here: https://doi.org/10.1101/2024.11.10.622873.

Data Availability

All data, methods, and results of statistical analyses are reported in this paper or the associated Supplementary data. We welcome any specific inquiries.

References

1 Tsukita S, Tanaka H, Tamura A. 2019. The claudins: from tight junctions to biological systems. *Trends Biochem Sci*. 44:141–152.
2 Krause G, *et al*. 2008. Structure and function of claudins. *Biochim Biophys Acta*. 1778:631–645.
3 Hewitt KJ, Agarwal R, Morin PJ. 2006. The claudin gene family: expression in normal and neoplastic tissues. *BMC Cancer*. 6:186.
4 Koval M. 2013. Differential pathways of claudin oligomerization and integration into tight junctions. *Tissue Barriers*. 1:e24518.
5 Lal-Nag M, Morin PJ. 2009. The claudins. *Genome Biol*. 10:235.
6 Günzel D, Yu ASL. 2013. Claudins and the modulation of tight junction permeability. *Physiol Rev*. 93:525–569.
7 Piontek J, *et al*. 2008. Formation of tight junction: determinants of homophilic interaction between classic claudins. *FASEB J*. 22:146–158.
8 Hempel C, *et al*. 2020. Assembly of tight junction strands: claudin-10b and claudin-3 form homo-tetrameric building blocks that polymerise in a channel-independent manner. *J Mol Biol*. 432:2405–2427.
9 Tokumasu R, *et al*. 2016. Dose-dependent role of claudin-1 in vivo in orchestrating features of atopic dermatitis. *Proc Natl Acad Sci U S A*. 113:E4061–E4068.
10 Meertens L, *et al*. 2008. The tight junction proteins claudin-1, -6, and -9 are entry cofactors for hepatitis C virus. *J Virol*. 82:3555–3560.

11 Greene C, Hanley N, Campbell M. 2019. Claudin-5: gatekeeper of neurological function. *Fluids Barriers CNS*. 16:3.
12 Wakayama E, *et al.* 2022. Modifying the blood–brain barrier by targeting claudin-5: safety and risks. *Ann N Y Acad Sci*. 1514: 62–69.
13 Katahira J, *et al.* 1997. *Clostridium perfringens* enterotoxin utilizes two structurally related membrane proteins as functional receptors *in vivo*. *J Biol Chem*. 272:26652–26658.
14 Katahira J, Inoue N, Horiguchi Y, Matsuda M, Sugimoto N. 1997. Molecular cloning and functional characterization of the receptor for *Clostridium perfringens* enterotoxin. *J Cell Biol*. 136: 1239–1247.
15 Veshnyakova A, *et al.* 2010. On the interaction of *Clostridium perfringens* enterotoxin with claudins. *Toxins (Basel)*. 2:1336–1356.
16 Kominsky SL, *et al.* 2004. *Clostridium perfringens* enterotoxin elicits rapid and specific cytolysis of breast carcinoma cells mediated through tight junction proteins claudin 3 and 4. *Am J Pathol*. 164:1627–1633.
17 Pahle J, *et al.* 2021. Effective oncoleaking treatment of pancreatic cancer by claudin-targeted suicide gene therapy with *Clostridium perfringens* enterotoxin (CpE). *Cancers (Basel)*. 13:4393.
18 Torres JB, *et al.* 2020. Radiolabeled cCpE peptides for SPECT imaging of claudin-4 overexpression in pancreatic cancer. *J Nucl Med*. 61:1756–1763.
19 Abuazza G, *et al.* 2006. Claudins 6, 9, and 13 are developmentally expressed renal tight junction proteins. *Am J Physiol Renal Physiol*. 291:F1132–F1141.
20 Du H, Yang X, Fan J, Du X. 2021. Claudin 6: therapeutic prospects for tumours, and mechanisms of expression and regulation (review). *Mol Med Rep*. 24:677.
21 Nakano Y, *et al.* 2009. A claudin-9-based ion permeability barrier is essential for hearing. *PLoS Genet*. 5:e1000610.
22 Krug SM, *et al.* 2012. Claudin-17 forms tight junction channels with distinct anion selectivity. *Cell Mol Life Sci*. 69:2765–2778.
23 Dimke H, *et al.* 2023. Claudin-19 localizes to the thick ascending limb where its expression is required for junctional claudin-16 localization. *Ann N Y Acad Sci*. 1526:126–137.
24 Colegio OR, Van Itallie CM, McCrea HJ, Rahner C, Anderson JM. 2002. Claudins create charge-selective channels in the paracellular pathway between epithelial cells. *Am J Physiol Cell Physiol*. 283: C142–C147.
25 Li G, *et al.* 2014. Knockout mice reveal key roles for claudin 18 in alveolar barrier properties and fluid homeostasis. *Am J Respir Cell Mol Biol*. 51:210–222.
26 Sweerus K, *et al.* 2017. Claudin-18 deficiency is associated with airway epithelial barrier dysfunction and asthma. *J Allergy Clin Immunol*. 139:72–81.e1.
27 Luo J, *et al.* 2018. CLDN18.1 attenuates malignancy and related signaling pathways of lung adenocarcinoma in vivo and in vitro. *Int J Cancer*. 143:3169–3180.
28 Hayashi D, *et al.* 2012. Deficiency of claudin-18 causes paracellular H+ leakage, up-regulation of interleukin-1β, and atrophic gastritis in mice. *Gastroenterology*. 142:292–304.
29 Sahin U, *et al.* 2008. Claudin-18 splice variant 2 is a pan-cancer target suitable for therapeutic antibody development. *Clin Cancer Res*. 14:7624–7634.
30 Li J. 2021. Targeting claudins in cancer: diagnosis, prognosis and therapy. *Am J Cancer Res*. 11:3406–3424.
31 Greene C, Campbell M. 2016. Tight junction modulation of the blood brain barrier: CNS delivery of small molecules. *Tissue Barriers*. 4:e1138017.
32 Erramilli SK, Dominik PK, Ogbu CP, Kossiakoff AA, Vecchio AJ. 2024. Structural and biophysical insights into targeting of claudin-4 by a synthetic antibody fragment. *Commun Biol*. 7:733.
33 Robertson SL, McClane BA. 2011. Interactions between *Clostridium perfringens* enterotoxin and claudins. *Methods Mol Biol*. 762:63–75.
34 Ogbu CP, Roy S, Vecchio AJ. 2022. Disruption of claudin-made tight junction barriers by *Clostridium perfringens* enterotoxin: insights from structural biology. *Cells*. 11:903.
35 Takahashi A, *et al.* 2011. Mutated C-terminal fragments of *Clostridium perfringens* enterotoxin have increased affinity to claudin-4 and reversibly modulate tight junctions in vitro. *Biochem Biophys Res Commun*. 410:466–470.
36 Saitoh Y, *et al.* 2015. Structural insight into tight junction disassembly by *Clostridium perfringens* enterotoxin. *Science*. 347: 775–778.
37 Shinoda T, *et al.* 2016. Structural basis for disruption of claudin assembly in tight junctions by an enterotoxin. *Sci Rep*. 6:33632.
38 Nakamura S, *et al.* 2019. Morphologic determinant of tight junctions revealed by claudin-3 structures. *Nat Commun*. 10:816.
39 Vecchio AJ, Stroud RM. 2019. Claudin-9 structures reveal mechanism for toxin-induced gut barrier breakdown. *Proc Natl Acad Sci U S A*. 116:17817–17824.
40 Vecchio AJ, Rathnayake SS, Stroud RM. 2021. Structural basis for *Clostridium perfringens* enterotoxin targeting of claudins at tight junctions in mammalian gut. *Proc Natl Acad Sci U S A*. 118: e2024651118.
41 Winkler L, *et al.* 2009. Molecular determinants of the interaction between *Clostridium perfringens* enterotoxin fragments and claudin-3. *J Biol Chem*. 284:18863–18872.
42 Fujita K, *et al.* 2000. *Clostridium perfringens* enterotoxin binds to the second extracellular loop of claudin-3, a tight junction integral membrane protein. *FEBS Lett*. 476:258–261.
43 Shrestha A, McClane BA. 2013. Human claudin-8 and -14 are receptors capable of conveying the cytotoxic effects of *Clostridium perfringens* enterotoxin. *mBio*. 4:e00594-12.
44 Sonoda N, *et al.* 1999. *Clostridium perfringens* enterotoxin fragment removes specific claudins from tight junction strands. *J Cell Biol*. 147:195–204.
45 Saeki R, *et al.* 2009. A novel tumor-targeted therapy using a claudin-4-targeting molecule. *Mol Pharmacol*. 76:918–926.
46 Simske JS. 2013. Claudins reign. *Tissue Barriers*. 1:e25502.
47 Adato A, *et al.* 2002. USH3A transcripts encode clarin-1, a four-transmembrane-domain protein with a possible role in sensory synapses. *Eur J Hum Genet*. 10:339–350.
48 Suzuki H, *et al.* 2014. Crystal structure of a claudin provides insight into the architecture of tight junctions. *Science*. 344:304–307.
49 Shinoda T, *et al.* 2016. Cell-free methods to produce structurally intact mammalian membrane proteins. *Sci Rep*. 6:30442.
50 Orlando BJ, *et al.* 2022. Development, structure, and mechanism of synthetic antibodies that target claudin and *Clostridium perfringens* enterotoxin complexes. *J Biol Chem*. 298:102357.
51 Nsairat H, *et al.* 2022. Liposomes: structure, composition, types, and clinical applications. *Heliyon*. 8:e09394.
52 Sligar SG, Denisov IG. 2021. Nanodiscs: a toolkit for membrane protein science. *Protein Sci Publ Protein Soc*. 30:297–315.
53 Belardi B, *et al.* 2019. Claudin-4 reconstituted in unilamellar vesicles is sufficient to form tight interfaces that partition membrane proteins. *J Cell Sci*. 132:jcs221556.
54 Cummins PM. 2012. Occludin: one protein, many forms. *Mol Cell Biol*. 32:242–250.

55 Saito AC, *et al.* 2021. Occludin and tricellulin facilitate formation of anastomosing tight-junction strand network to improve barrier function. *Mol Biol Cell*. 32:722–738.

56 Severson EA, Parkos CA. 2009. Structural determinants of Junctional Adhesion Molecule A (JAM-A) function and mechanisms of intracellular signaling. *Curr Opin Cell Biol*. 21:701–707.

57 Otani T, *et al.* 2019. Claudins and JAM-A coordinately regulate tight junction formation and epithelial polarity. *J Cell Biol*. 218: 3372–3396.

58 Laukoetter MG, *et al.* 2007. JAM-A regulates permeability and inflammation in the intestine in vivo. *J Exp Med*. 204:3067–3076.

59 Li J, Parker B, Martyn C, Natarajan C, Guo J. 2013. The PMP22 gene and its related diseases. *Mol Neurobiol*. 47:673–698.

60 Nicolas WJ, *et al.* 2025. Structure of the lens MP20 mediated adhesive junction. *Nat Commun*. 16:2977.

61 Nelson KS, Furuse M, Beitel GJ. 2010. The Drosophila claudin Kune-kune is required for septate junction organization and tracheal tube size control. *Genetics*. 185:831–839.

62 Varadi M, *et al.* 2024. AlphaFold Protein Structure Database in 2024: providing structure coverage for over 214 million protein sequences. *Nucleic Acids Res*. 52:D368–D375.

63 Shrestha A, *et al.* 2022. Characterizing the contributions of various *Clostridium perfringens* enterotoxin properties to *in vivo* and *in vitro* permeability effects. *mSphere*. 7:e0027622.

64 Fernández Miyakawa ME, Pistone Creydt V, Uzal FA, McClane BA, Ibarra C. 2005. Clostridium perfringens enterotoxin damages the human intestine in vitro. *Infect Immun*. 73:8407–8410.

65 Becker A, *et al.* 2018. Functionalization of gold-nanoparticles by the *Clostridium perfringens* enterotoxin C-terminus for tumor cell ablation using the gold nanoparticle-mediated laser perforation technique. *Sci Rep*. 8:14963.

66 Van Itallie CM, Lidman KF, Tietgens AJ, Anderson JM. 2019. Newly synthesized claudins but not occludin are added to the basal side of the tight junction. *Mol Biol Cell*. 30:1406–1424.

67 Ölander M, Wiśniewski JR, Matsson P, Lundquist P, Artursson P. 2016. The proteome of filter-grown Caco-2 cells with a focus on proteins involved in drug disposition. *J Pharm Sci*. 105:817–827.

68 Rathnayake SS, Erramilli SK, Kossiakoff AA, Vecchio AJ. 2024. Cryo-EM structures of Clostridium perfringens enterotoxin bound to its human receptor, claudin-4. *Structure*. 32: 1936–1951.e5.

69 Nunes FD, *et al.* 2006. Distinct subdomain organization and molecular composition of a tight junction with adherens junction features. *J Cell Sci*. 119:4819–4827.

70 Zhao J, *et al.* 2018. Multiple claudin-claudin cis interfaces are required for tight junction strand formation and inherent flexibility. *Commun Biol*. 1:50.

71 Suzuki H, Tani K, Tamura A, Tsukita S, Fujiyoshi Y. 2015. Model for the architecture of claudin-based paracellular ion channels through tight junctions. *J Mol Biol*. 427:291–297.

72 Nagarajan SK, Klein S, Fadakar BS, Piontek J. 2023. Claudin-10b cation channels in tight junction strands: octameric-interlocked pore barrels constitute paracellular channels with low water permeability. *Comput Struct Biotechnol J*. 21:1711–1727.

73 UniProt Consortium. 2023. UniProt: the Universal Protein Knowledgebase in 2023. *Nucleic Acids Res*. 51:D523–D531.

74 Notredame C, Higgins DG, Heringa J. 2000. T-Coffee: a novel method for fast and accurate multiple sequence alignment. *J Mol Biol*. 302:205–217.

75 Madeira F, *et al.* 2022. Search and sequence analysis tools services from EMBL-EBI in 2022. *Nucleic Acids Res*. 50:W276–W279.

76 Waterhouse AM, Procter JB, Martin DMA, Clamp M, Barton GJ. 2009. Jalview version 2—a multiple sequence alignment editor and analysis workbench. *Bioinformatics*. 25:1189–1191.

77 Schlebach JP, *et al.* 2013. Reversible folding of human peripheral myelin protein 22, a tetraspan membrane protein. *Biochemistry*. 52:3229–3241.

78 Stefanski KM, *et al.* 2022. How T118M peripheral myelin protein 22 predisposes humans to Charcot–Marie–Tooth disease. *J Biol Chem*. 299:102839.

79 Punjani A, Rubinstein JL, Fleet DJ, Brubaker MA. 2017. Brubaker, cryoSPARC: algorithms for rapid unsupervised cryo-EM structure determination. *Nat Methods*. 14:290–296.

80 Pettersen EF, *et al.* 2004. UCSF Chimera–a visualization system for exploratory research and analysis. *J Comput Chem*. 25: 1605–1612.